# A Study of Contact Models for Slider-Disk Contact and Impact

**Du Chen and David B. Bogy**

Computer Mechanics Laboratory

Dept. of Mechanical Engineering

University of California

Berkeley, CA 94720

## ABSTRACT

The slider-disk impact and contact need to be properly modeled in the air bearing slider dynamic simulator in order to accurately analyze the dynamics of contact or partial contact sliders for $1T/in^2$ or higher recording densities in hard disk drives. Static contact models, such as asperity-based contact models and the contact model based on influence coefficients, can be used to model the slider-disk contact and impact, since the contact and impact between the slider and the disk are quasi-static. The limitations of these models are discussed and the algorithms used for applying these models to the slider dynamic simulation are analyzed, in order to efficiently use them in the simulation. Other contact models, such as the multi-asperity contact model proposed by Cha and Bogy [1] in the current CML air bearing program and the contact model proposed by Iida and Ono [2] in their simulations for contact and near-contact sliders are also discussed in this report.

## INTRODUCTION

The slider-disk spacing has to decrease to less than 3nm for 1Tbit/in$^2$ magnetic recording density, causing the slider to contact or impact the disk. In the contact head disk interface design, the slider's trailing edge is expected to contact the disk surface during the head reading and writing process. So the slider-disk impact and contact need to be properly modeled in the air bearing slider dynamic simulator in order to accurately analyze the dynamics of these contact or partial contact sliders.

The slider-disk contact and impact models should be simple and accurate and have an efficient numerical algorithm. In the CML slider dynamic simulator the Newmark-Beta method is used to solve the slider-disk interface dynamic equations [3]. The time step is at most $10^{-6}$ sec due to the high frequency of the slider's motion. This means at least $10^3$ time steps for only 1ms of motion. When the slider contacts the disk, the simulator needs to solve for the slider-disk contact force several times as well as solving the dynamic Reynolds Equations for the air bearing pressure, until the entire system of the slider's motion equations converge at every time step. Hence the slider dynamic simulation needs a numerically efficient model for the slider-disk impact and contact.

In the early simulators the coefficient of restitution model of the slider-disk impact was used to calculate the approximate impact force and the speed of the slider after impact [4]. Another common way has been to use the contact stiffness and damping for the calculation of the slider-disk impact force [5]. These two methods are very convenient for computation, but it is very difficult to obtain the required coefficient of restitution or contact stiffness and damping coefficients for a 3-D slider-disk contact. Also the coefficient of restitution cannot give the contact duration and the contact force at the

same time. Later several static contact models were applied to the simulation, for example, the Greenwood-Williamson (GW) model [6], CEB model [7] and KE model [8]. All of these models belong to the class of asperity-based contact models. Cha and Bogy proposed a multiple asperity-based impact model [1], which is based on Chang and Ling's elastic-plastic model [9]. Peng et al [10] used an elastic contact model based on influence coefficients to simulate the slider-disk contact. Iida and Ono [2] numerically calculated the contact force considering the asperity contact and the deformation of the base plane of each asperity due to the bulk deformation. Influence coefficients are used in their model to calculate the deformation of each asperity's base plane. Although the finite element method (FEM) is adequate in solving elastic-plastic contact problems with acceptable accuracy [11] [12], its requirement for a large number of elements reduces its effectiveness in analyzing surface contact with a practical size system. Its high computation cost makes it almost impossible to use the FEM to analyze the slider-disk contact in the slider dynamic simulation.

Currently the CML air bearing program uses the GW model and CEB model (also called elastic-plastic model, i.e. EP model) for the slider-disk asperity contact, which occurs when the gap between the slider and the disk is less than the glide height but higher than zero, and it uses Cha's model [1] for the crash contact, which happens when the slider-disk gap is less than zero. In this report we analyze all of these contact models, i.e. the asperity-based models and the elastic model with influence coefficients. Their applications and limitations to the slider dynamic simulation are examined. Finally a preferred approach for the simulation of the slider-disk contact and impact is proposed.

## QUASI-STATIC IMPACT

The CML slider dynamic simulation shows that when the slider impacts the disk the impact speed of the slider is on the order of $10^{-1}$m/s, which is much less than the elastic wave speeds in the slider and the disk. The sliding speed of the slider with respect to the disk, which is proportional to the disk rotation speed and the radius position of the slider, is on the order of $10^{1}$m/s. This value is also much smaller than the elastic wave speeds. So the slider-disk impact is quasi-static, which means that the deformation is restricted to the vicinity of the contact area and can be obtained using the static contact theory with the elastic wave motion in the bodies ignored. So we can use static contact models to approximate the slider-disk contact. In fact the asperity-based contact models, such as the GW model and the CEB model used by Hu [3] in the slider dynamic simulation and the KE model used by Suh and Polycarpou [13] for their two dimensional slider simulation, are all static contact models, as is Cha's multi-asperity contact model [1]. The influence coefficient model of contact is based on static linear elasticity and it can also be used as a quasi-static impact model.

## DECOUPLED NORMAL PRESSURE AND TANGENTIAL FRICTION

In the quasi-static slider-disk contact problem the normal pressure and the friction traction can be decoupled without significant loss of accuracy. Johnson [14] showed analytically that the influence of frictional traction on the normal pressure is very small for a sliding punch over the surface of a half-space with a friction coefficient 0.5. The friction coefficient between the slider and the disk is usually less than 0.5 due to the lubricant and carbon overcoat. And the default value used in CML simulation is 0.3. So

we can employ the contact models to obtain the contact force and then obtain the friction force through Coulomb's law with a constant friction coefficient.

## ASPERITY-BASED CONTACT MODELS

### Nomenclature

$A_n$ nominal contact area

$A$ real contact erea

$d$ separation based on mean asperity heights

$d^*$ normalized separation ($d^* = \frac{d}{\sigma_s}$)

$E_s$ Young's modulus of the slider

$E_d$ Young's modulus of the disk

$E$ Hertz elastic modulus ($E = (\frac{1-v_s^2}{E_s} + \frac{1-v_d^2}{E_d})^{-1}$)

$H$ hardness of the softer material

$K$ hardness factor ($K = 0.454 + 0.410v$)

$N$ total number of asperities

$P$ total contact force

$R$ asperity radius of curvature

$t$ lubricant thickness

$u$ height of an asperity measured from the mean of asperity heights

$u^*$ normalized asperity height ($u^* = \frac{u}{\sigma_s}$)

$y_s$ distance between the mean of asperity heights and the mean of surface heights

$\eta$ area density of asperities

$v$ Poisson's ratio of the softer material among the slider and the disk

$v_s$ Poisson's ratio of the slider

$v_d$ Poisson's ratio of the disk

$\sigma$ standard deviation of surface height

$\sigma_s$ standard deviation of asperity height

$\omega$ contact interference of an asperity

$\omega_c$ critical interference at the inception of plastic deformation inside the asperity

$\psi$ plasticity index

## 1. Introduction

The asperity-based contact models are based on the incorporation of a single asperity contact in a statistical model of multiple asperity contacts. The contact of two rough surfaces can be modeled by an equivalent single rough surface contacting a flat rigid plane, as proved by Greenwood and Tripp [15]. For the equivalent rough surface five assumptions are usually adopted in an asperity-based model.

(1) The rough surface is isotropic.

(2) The asperities have the same simple geometry near their summits, for example the asperities are spherical or ellipsoidal.

(3) The asperity heights vary randomly but follow a probability distribution, for example, a Gaussian distribution etc.

(4) Asperities deform due to the contact with the rigid surface. But asperities are far apart and interactions between them are negligible.

(5) Bulk deformation is also negligible.

The first asperity-based contact model was presented in the pioneering work of Greenwood and Williamson (GW model) [6]. It is based on the Hertz elastic contact solution for a single elastic spherical asperity. So it is mainly valid for purely elastic contact. Much earlier some purely plastic contact models were proposed by Abbott and Firestone [16]. They were extended to asperity-based contact models for purely plastic contact. To bridge the gap between the purely elastic and the purely plastic contact, Chang et al [7] proposed the CEB model by introducing a critical interference ($\omega_c$), above which an elastic contacting asperity turns to a fully plastic deformation. This fully plastically deformed asperity is assumed to have a uniform distribution of contact pressure and conserve the volume of the asperity tip. However, this simplification causes a discontinuity in the contact load at the transition from elastic to elastic-plastic contact. Evseev, et al [17], Chang [18] and Zhao, et al [19] proposed various mathematical modifications to smooth the discontinuity. Kogut and Etsion [8] incorporated an elastic-plastic FEM solution to the contact of a sphere and revised the CEB elastic-plastic model to the KE model, which does not have the discontinuity.

The GW model, CEB model and KE model are typical asperity-based contact models that assume that the asperities are spheres with the same radius and the asperity heights are normally distributed. McCool [20] relaxed these two assumptions and treated the rough surface as anisotropic with a random distribution of asperity radii. However the results showed good agreement with those of the simple GW model. The GW model and CEB model, because of their simplicity, were extended to different asperity geometries and asperity height distributions, Horng [21], Kogut and Estion [22], Yu and Polycarpou [23]. Also other modifications of these models were made, for example, the modification

with a varying hardness by Jackson and Green [24]. However these papers [21-24] fail to show that the two simple assumptions of the GW, CEB and KE models produce results that deviate from real contact interfaces. In this report we accept the assumptions of simple spherical asperities and Gaussian distribution of asperity heights and compare the three typical probabilistic models, i.e. the GW model, CEB model and KE model.

Obviously Assumptions (4) and (5) limit the applicability of the asperity-based contact models. When the surface separation is less than 0, the asperities can undergo large deformations which may violate Assumption (4). For higher values of average contact pressure bulk deformation may occur, which violates Assumption (5). So asperity-based contact models are valid only when surface separation $d > 0$ and nominal contact pressure $\overline{p} << H$ .

## 2. Surface roughness parameters

In these three models, a rough surface is described by the standard deviation of asperity heights, the radius of curvature of their summits and the areal density of the asperities. McCool [25] showed a systematic way to obtain these parameters from the surface profile *z(x)* with an assumption that *z(x)* is a Gaussian random variable. Three spectral moments of the profile *z(x)* can be defined as,

$$m_0 = AVG[z^2],\ m_2 = AVG[(\frac{dz}{dx})^2],\ m_4 = AVG[(\frac{d^2z}{dx^2})^2]. \tag{1}$$

Two isotropic rough surfaces in contact can be replaced by an equivalent rough surface contacting a rigid flat surface. Then three spectral moments of the equivalent rough surface are,

$$m_0 = (m_0)_1 + (m_0)_2,\ m_2 = (m_2)_1 + (m_2)_2,\ m_4 = (m_4)_1 + (m_4)_2. \tag{2}$$

Obviously $m_0$ is the variance of surface heights, i.e., the surface height standard deviation $\sigma = (m_0)^{1/2}$. The radius of curvature, the asperity density, and the asperity height standard deviation can be expressed as,

$$R = 0.375(\frac{\pi}{m_4})^{1/2},\ \eta = \frac{\mathrm{m}_4}{6\pi\sqrt{3}m_2},\ \sigma_s = \sqrt{\sigma^2 - \frac{3.717\times10^{-4}}{\eta^2 r^2}}\ . \tag{3}$$

In a strict mathematical sense the above equations have only been proved for Gaussian random surfaces [26]. They are not valid for a Weibull random surface. So using a non-Gaussian asperity height distribution with the above equations [23] has not been validated.

These three parameters, i.e. radius of curvature, asperity density, and asperity height standard deviation, are scale-dependent. In fact the surface topography is not a stationary random process and the three spectral moments of the height distribution depend on the length of the statistical sample [27]. This means that instruments with different resolutions and scan lengths yield different values of these statistical parameters for the same surface. Majumdar and Bhushan [28] analyzed their dependence on the spatial resolution and surface magnification for a magnetic tape surface and a magnetic disk surface. They proposed a new contact model in which the rough surfaces are characterized by fractal geometry [29]. After that several contact analyses of elastic-plastic fractal surfaces were proposed [30] [31]. All of these analyses retain assumption (4) and assumption (5), and they did not cite any experimental work as a proof that fractal contact models are superior to asperity-based contact models.

## 3. A proper model for slider disk asperity contact

As mentioned above, the GW model is valid for purely elastic contact, the CEB model is a rough extension to elastic-plastic contact and the KE model is a more accurate elastic-plastic model based on the FEM analysis, but with the cost of much more complicated expressions. For specified rough surfaces all three of these models give the contact load and the real contact area as functions of the surface separation d, where, in fact, *d=FH-ys*, or *d=FH-ys-t* if a lubricant thickness *t* is considered.

GW model

$$P(d) = \frac{2}{3}(\pi RKH\omega_c)(A_n\eta)\int_d^{\infty} I^{1.5} \tag{4}$$

$$A(d) = (\pi R\omega_c)(A_n\eta)\int_d^{\infty} I^{1} \tag{5}$$

CEB model

$$P(d) = \frac{2}{3}(\pi RKH\omega_c)(A_n\eta)(\int_d^{d+\omega_c} I^{1.5} + 1.5\int_{d+\omega_c}^{\infty}(2-\frac{\omega_c}{u-d})I^{1}) \tag{6}$$

$$A(d) = (\pi R\omega_c)(A_n\eta)(\int_d^{d+\omega_c} I^{1} + \int_{d+\omega_c}^{d+6\omega_c}(2-\frac{\omega_c}{u-d})I^{1}) \tag{7}$$

KE model

$$P(d) = \frac{2}{3}(\pi RKH\omega_c)(A_n\eta)(\int_d^{d+\omega_c} I^{1.5} + 1.03\int_{d+\omega_c}^{d+6\omega_c} I^{1.425} + 1.4\int_{d+6\omega_c}^{d+110\omega_c} I^{1.263} + \frac{3}{K}\int_{d+110\omega_c}^{\infty} I^{1}) \tag{8}$$

$$A(d) = (\pi R\omega_c)(A_n\eta)(\int_d^{d+\omega_c} I^{1} + 0.93\int_{d+\omega_c}^{d+6\omega_c} I^{1.136} + 0.94\int_{d+6\omega_c}^{d+110\omega_c} I^{1.146} + 2\int_{d+110\omega_c}^{\infty} I^{1}) \tag{9}$$

where, $I^{\alpha} = (\frac{u-d}{\omega_c})^{\alpha}\phi(u)du$

$= (\frac{u-d}{\omega_c})^{\alpha}\frac{1}{\sqrt{2\pi}\sigma_s}\exp(-\frac{u^2}{2\sigma_s^{\,2}})du,$ for the Gaussian distribution.

The CEB model assumes the asperities are either elastically deformed ($\omega < \omega_c$) or fully plastically deformed ($\omega \geq \omega_c$), with the corresponding two terms on the right hand sides

of Equations (6) and (7). However, the KE model uses the FEM results and asserts that asperities have four different deformation states. They are elastically deformed asperities ($\omega < \omega_c$), elastic-plastically deformed asperities with a plastic region under the contact interface ($\omega_c \le \omega < 6\omega_c$), elastic-plastically deformed asperities with a plastic annulus on the contact interface ($6\omega_c \le \omega < 110\omega_c$), and fully plastically deformed asperities ($\omega \ge 110\omega_c$). These four states correspond to the four terms on the right hand sides of Equations (8) and (9).

Although Equations (4-9) have many variables, they can be reduced to functions of the separation d and the plasticity index Ψ. The plasticity index, which is defined by Greenwood and Williamson and expressed as $\psi = (\frac{\omega_c}{\sigma_s})^{-1/2}$, determines the main deformation state of the contacting asperities, i.e. elastic, elastic-plastic, or plastic. Fig. 1 shows the distribution function of asperity heights. All of the asperities with heights larger than the separation are in contact as shown as a dark region in Fig. 1. All of the asperities with heights larger than the critical interference plus the separation are in elastic-plastic or plastic deformation. It is obvious that if the separation is larger than $3\sigma s$, the number of asperities in contact is negligible and in fact the surfaces are practically separated. The number of asperities in elastic-plastic deformation is $N\int_{\omega_c+d}^{\infty} \phi(u)du$. Here we have a restriction $d>0$ so that the assumption (4) is valid. It is found that the above number of asperities in elastic-plastic deformation is negligible if the critical interference is less than 3σs, which corresponds to $\Psi<0.58$. This is consistent with Greenwood and

Williamson's comment [6] that when $\Psi<0.6$ plastic contact could be caused only if the nominal pressure between two surfaces were very large. Similarly we conclude,

(1) The contacting asperities are mainly in elastic deformation if $\Psi<0.58$, i.e. $\omega_c > 3\sigma_s$.

(2) The number of plastically deformed asperities is negligible if $\Psi<6.06$, i.e. $110\omega_c > 3\sigma_s$.

(3) If $0.58<\Psi<1.41$, i.e. $\omega_c < 3\sigma_s < 6\omega_c$, the number of elastic-plastically deformed asperities with plastic annulus on the contact interface is negligible, but the elastic-plastically deformed asperities with a plastic region below the contact interface needs to be considered.

So if $\Psi<1.41$ the asperities are mainly in elastic deformation or elastic-plastic deformation with a plastic region below the contact interface, which corresponds to the first two terms in Equations (8) and (9). Notice that the term in (8) $1.03\int_{d+\omega_c}^{d+6\omega_c} I^{1.425}$ is close to $1.00\int_{d+\omega_c}^{d+6\omega_c} I^{1.5}$ and the term in (9) $0.93\int_{d+\omega_c}^{d+6\omega_c} I^{1.136}$ is also be close to $1.00\int_{d+\omega_c}^{d+6\omega_c} I^{1}$. So we may expect that the KE model produces results close to those produced by the GW model for $\Psi<1.41$.

Numerical results of three $\Psi$ cases of the slider-disk contact are obtained using the GW model, CEB model and KE model. These three cases have typical slider and disk roughnesses and material parameters [13], as shown in Table I, and produce $\psi = 0.836,\ 0.587,$ and $0.386$. The contact load versus the separation and the contact area versus the separation are plotted for each $\Psi$ for these three models, respectively. As shown in Fig. 2, the difference between the results of these three models

is very small except that for case 1, where for separation less than 1nm the result of the CEB model deviates from those of the GW model and KE model. In case 1 $\psi$ =*0.836*, the asperities are either in elastic deformation or in elastic-plastic deformation with plastic regions below the contact interface. The CEB model just assumes all of the elastic-plastically deformed asperities are in fully plastic deformation, while the contact force and contact area of these elastic-plastically deformed asperities are much closer to those of elastically deformed asperities. This is the reason why it gives different results. So the CEB model may not be accurate for the slider-disk contact analysis with large $\psi$ and small separation.

For slider-disk asperity contact, if the material constants $E$ is 85.29GPa, $H$ is 2.5GPa, and $\nu$ is 0.2, the roughness parameters $\sigma_s$ is less than 2 nm and R is of the order of 1 μm, then we can expect the plasticity index $\psi = (\frac{\omega_c}{\sigma_s})^{-1/2} = \frac{2E}{\pi KH}(\frac{\sigma_s}{R})^{1/2}$ to be around 1. So the contacting asperities are mainly in elastic or elastic-plastic deformation. The difference between the GW model and the KE model is expected to be very small for slider-disk asperity contact. For simplicity we will use the GW contact model in the slider's dynamic simulation. If the slider-disk contact has $\Psi$*>0.58*, we can turn to the KE model for better accuracy, but the GW model is still a good approximation. However, the CEB model is not applicable to the slider-disk contact with $\Psi$*>0.58*, which has been shown in the above slider-disk asperity contact cases.

## 4. Numerical implementation of the GW model and the KE model

Notice that all of the terms in the Equations (4), (5), (8), and (9) have the following form,

$$\int_{l(d,\omega_c)}^{u(d,\omega_c)} I^{\alpha} = \int_{l(d,\omega_c)}^{u(d,\omega_c)} (\frac{u-d}{\omega_c})^{\alpha} \frac{1}{\sqrt{2\pi}\sigma_s} \exp(-\frac{u^2}{2\sigma_s{}^2}) du$$

$$= (\frac{\sigma_s}{\omega_c})^{\alpha} \int_{l(d,\omega_c)}^{u(d,\omega_c)} (\frac{u-d}{\sigma_s})^{\alpha} \frac{1}{\sqrt{2\pi}\sigma_s} \exp(-\frac{u^2}{2\sigma_s{}^2}) du \tag{10}$$

$$= \psi^{2\alpha} \int_{l(d^*,\psi)}^{u(d^*,\psi)} (u^* - d^*)^{\alpha} \frac{1}{\sqrt{2\pi}} \exp(-\frac{u^{*2}}{2}) du^*,$$

where $u(d,\omega_c)$ and $l(d,\omega_c)$ are the upper and lower bounds of the integration, respectively.

As seen from Equation (10), the integral is expressed as a function of d if $\Psi$ is fixed. So in the GW model and the KE model the contact load and contact area are only functions of the separation if the plasticity index is fixed.

To avoid the integration process at each time step, a table look-up method can be used in the computation. These tables are composed of all the integration results for various values of $d^*$. For the GW model the upper bound and lower bound in Equation (10) are independent of $\Psi$, so the tables can be predetermined. For the KE model the upper bound and lower bound in Equation (10) depend on $\Psi$. So the look-up tables have to be established in the program for different input values of $\Psi$. The improper integrals, which have $\infty$ as an upper bound, are approximated by proper integrals. Fig. 1 shows that the density function of the Gaussian distribution, i.e. $\frac{1}{\sqrt{2\pi}\sigma_s} \exp(-\frac{u^2}{2\sigma_s{}^2})$, decreases to near zero extremely fast as $u$ increases beyond $3\sigma_s$. So when the upper bound of integration in equation (10) is infinity, the upper bound can be taken as a sufficiently large number, for example $3\sigma_s$ or $6\sigma_s$, without significant loss of accuracy. The Romberg method [32] is used to calculate the proper integrals for the tables, instead of the numerical integration method currently in the CML air bearing code, which often does not converge.

Meshing the slider ABS is required in order to apply the asperity based contact model to the slider-disk asperity contact. Due to the pitch and roll of the slider motion and the air bearing surface (ABS) design, the slider surface is not parallel to the disk. The slider ABS is meshed into grids in the simulation. Each grid on the ABS is assumed to have a uniform separation from the disk and the slider-disk contact force and contact area are decretized as step functions. The GW model or the KE model is applied to each grid to obtain the contact load and contact area. Then the total contact load and contact area are the summation of the contact load and contact area of all grids. The table look-up method can speed up this process. In the CML air bearing simulation an adaptive grid generation based on the air pressure gradient is used to numerically solve the Reynolds Equation [33]. In this adaptive mesh the grid density is higher at ABS regions where the flying height is lower. Also those places with lower flying heights are more likely to contact the disk. We can also use this adaptive mesh to analyze the slider-disk asperity contact in the slider dynamic simulation. This avoids introducing another mesh into the simulation.

Both contact force and contact area are nonlinear functions of separation. So the effects of pitch and roll on the contact force and contact area are not negligible even for pitch and roll angles on the order of microradians. Fig. 3 shows plots of contact force versus pitch angle and contact area ratio versus pitch angle for rough slider and disk surfaces (case 1 in Table I) with a minimum separation of 2nm. Here the tailing pad of the slider is a $30\mu m \times 30\mu m$ square and it is in asperity contact with the disk. We can see that the GW model and the KE model give the same results and that the contact force and contact area strongly depend on the pitch angle. We may also expect that the roll angle has a similar effect on the contact force and contact area. But the effect of the roll angle is

less than that of the pitch angle, since the roll angle is much smaller than the pitch angle. The slider-disk contact simulation by Suh and Polycarpou [13] neglected the effect of the pitch and roll and only considered the effect of the contact pad area, i.e. norminal contact area $A_n$, upon the total contact force. This may not be accurate in some cases.

## 5. Asperity-based contact models relaxing Assumption (4) and (5)

There are several advanced asperity-based contact models that relax the last two assumptions of a typical asperity-based contact model, i.e. the assumption of no asperity interactions and the assumption of no bulk deformation. However, all of them are somewhat questionable.

For example, Zhao and Chang [34] proposed a model of asperity interactions in elastic-plastic contact of rough surfaces, which basically is a kind of asperity-based contact model. First they applied Saint-Venant's Principle of elasticity to equate the deformation at a given asperity due to pressures at all other contacting asperities shown in Fig. 4(a) to the deformation at that asperity due to an equivalent uniform pressure applied over the surface area outside the region of that asperity shown in Fig. 4(b). However, Saint-Venant's Principle is at best valid only for the strain and stress of a given point remote from loading regions. So it can not validate the equivalence of the two situations shown in Fig. 4. To consider the interactions between asperities, they used the linear elasticity theory and the influence coefficient (or Love's formula [35]) to calculate the deformation of a given asperity due to the forces at all other contacting asperities, while the deformation of all contacting asperities is assumed to be elastic-plastic in their model.

Iida and Ono [2] included the bulk deformation in their asperity-based elastic contact model for the simulation of contact and near-contact sliders. In their model, the

displacement of the tip of each asperity is composed of two parts. One part is due to the deformation of the tip of the given asperity under Hertzian contact and the other part is due to the deformation of the base plane of the given asperity under the asperity contact forces of all other contacting asperities. In this sense, for the contact of a rigid flat surface and a single spherical asperity on a half space, the displacement of the asperity tip is only due to the Hertzian contact between the rigid flat surface and the spherical asperity, which depends only on the Young's modulus of the asperity and the contact load. But suppose that Young's modulus of the half space is different from that of the spherical asperity. It is obvious that the displacement of the asperity tip increases as the Young's modulus of the half space decreases. So Iida and Ono's contact model is also questionable.

## CONTACT MODEL BASED ON INFLUENCE COEFFICIENTS

### 1. Introduction

This kind of contact model is based on linear elasticity analysis of loading on an isotropic elastic half-space. The influence coefficient comes from the effect of uniform pressure acting on a rectangular area as analyzed by Love [35]. The deflection of a general point (x, y) on the surface due to a uniform pressure $p$ acting on a rectangular area $2a \times 2b$ centered at the origin is given by Love's formula [35],

$$\bar{u}_z(x,y;a,b) = p \cdot$$
$$\frac{1-v^2}{\pi E}\{(x+a)\ln[\frac{(y+b)+\sqrt{(y+b)^2+(x+a)^2}}{(y-b)+\sqrt{(y-b)^2+(x+a)^2}}+(y+b)\ln[\frac{(x+a)+\sqrt{(y+b)^2+(x+a)^2}}{(x-a)+\sqrt{(y+b)^2+(x-a)^2}}]$$
$$+(x-a)\ln[\frac{(y-b)+\sqrt{(y-b)^2+(x-a)^2}}{(y+b)+\sqrt{(y+b)^2+(x-a)^2}}+(y-b)\ln[\frac{(x-a)+\sqrt{(y-b)^2+(x-a)^2}}{(x+a)+\sqrt{(y-b)^2+(x+a)^2}}]\}$$

$$= p\frac{1-\nu^2}{\pi E}c(x, y; a, b) \tag{11}$$

Here the function $c$ is called the influence coefficient, which relates the normal pressure in the rectangle with the size of $a \times b$ with the normal displacement at the point ($x$, $y$). Obviously $c$ is only a function of the position of the general point and the size of the rectangular area. Love also found expressions from which the stress components at a general point in the solid can be obtained. He commented that the component of shear stress theoretically becomes unbounded at the corners of the rectangle, but elsewhere all the stress components are bounded. These results are useful in the numerical solution of more general static contact problems of two bodies with uniformly loaded rectangles as "boundary elements". First, the normal and tangential tractions can be decoupled with only a small loss of precision by neglecting the effect of the tangential traction on the normal pressure, which arises when the materials of the two bodies are different. Then the discretized normal displacement of a contacting rough surface and the discretized normal pressure are related through the influence coefficients. Finally, the normal displacement of the contacting rough surface and the normal pressure are solved through numerical methods. This approach is described by Johnson [14].

For contact with a layered half space or contact in cases where the normal pressure and the tangential traction are coupled, the influence coefficient can be calculated using the FEM [36], where the influence of the applied unit load on the deflection at each node is analyzed through the FEM, or from the elasticity solution for a unit load on the surface of the half space [37], where the Papkovich-Neuber potentials are employed in a Fast Fourier analysis. However, the influence coefficient is still a function of the relative position and the size of the loading area.

## 2. Application to slider-disk contact

Several approximations are made to simplify the slider-disk contact problem. We need not consider the layered structure of the disk since we are not interested in the stress field in the disk. The disk is simply assumed to be a homogeneous isotropic half space. As discussed before, the normal pressure and the friction traction are decoupled without significant loss of accuracy. So the influence coefficient expressed in Equation (11) can be directly used. The slider and the projection of the slider on the disk are discretized into grids with the same mesh as shown Fig. 5. Each grid rectangle has a center node. The gap between the slider and the disk, the slider profile and the disk profiles, the contact pressure between the slider and the disk, and the elastic normal displacements of the slider and disk surfaces due to contact are all assumed to be uniform on each rectangular grid with the value evaluated at the center node. In another words, all of them are discretized to stepwise functions.

The slider-disk gap $h$ is the distance between the slider and disk profiles $Z_{(s)}$ and $Z_{(d)}$, i.e., $h = Z_{(s)} - Z_{(d)}$. In the slider dynamic simulation $h$ corresponds to the motion of the slider. $h_i \begin{cases} > 0, & \text{when node i is not in contact} \\ < 0, & \text{when node i is in contact} \end{cases}$

Provided there is no interpenetration, the elastic normal displacements of node $i$ on the slider $\overline{u}_{z(s)i}$ and the elastic displacement of the corresponding node on the disk $\overline{u}_{z(d)i}$, then satisfy the relationship,

$$\overline{u}_{z(s)i} + \overline{u}_{z(d)i} + h_i \begin{cases} = 0, & \text{within a contact region} \\ > 0, & \text{outside contact regions} \end{cases} \tag{12}$$

The influence coefficient $c_{ij}$ is used to express the displacement at node i due to a unit pressure element centered at node *j* acting on the rectangular grid. The total displacement at node *i* is then expressed by,

$$\bar{u}_{z(s)i} = \frac{1-v_s^{\,2}}{\pi E_s}\sum c_{ij(s)}p_j,\ \bar{u}_{z(d)i} = \frac{1-v_d^{\,2}}{\pi E_d}\sum c_{ij(d)}p_j\ , \tag{13}$$

where $c_{ij(s)}$ and $c_{ij(d)}$ are the influence coefficient on the slider and on the disk surface, respectively. If we also apply Equation (11) to the slider surface for $c_{ij(d)}$, then we can obtain a similar equivalence of the contact between two rough surfaces and the contact between a flat and a rough surface as in [15]. Explicitly the relative displacement can be expressed as,

$$\begin{aligned}\bar{u}_{z(s)i} + \bar{u}_{z(d)i} &= \frac{1-v_s^{\,2}}{\pi E_s}\sum c_{ij}p_j + \frac{1-v_d^{\,2}}{\pi E_d}\sum c_{ij}p_j \\ &= \sum\left(\frac{1-v_s^{\,2}}{\pi E_s} + \frac{1-v_d^{\,2}}{\pi E_d}\right)c_{ij}p_j \\ &= \sum C_{ij}p_j\ ,\end{aligned}$$

where $C_{ij} = \frac{1-v_s^{\,2}}{\pi E_s}c_{ij} + \frac{1-v_d^{\,2}}{\pi E_d}c_{ij} = \frac{1}{E^*}c_{ij}$.

Then Equation (12) can be expressed as,

$$\sum C_{ij}p_j \begin{cases} = -h_i, & \text{within a contact region} \\ > -h_i, & \text{outside contact regions,} \end{cases} \tag{14}$$

Here the $C_{ij}$'s form a matrix of the influence coefficients for the slider-disk contact interface and they define a linear system that relates the normal pressure to the elastic normal displacement. To simulate the slider dynamics, we need to solve the linear system and obtain the pressure elements. Notice that the pressure element $p_i$ should satisfy

$0 \le p_i \le H$ . The total contact load $P$ carried by the contact region is the sum of the pressure elements, i.e.

$P = \sum p_i s_i$ , where $s_i$ is the area of the grid at node i.

Obviously this elastic model with influence coefficients considers the interactions between nearby grids and the effect of bulk deformation. This model can simulate the contact between discretized real surfaces. However, this model is not applicable when a large number of contact nodes are plastically deformed, since the basis of the model is from linear elasticity theory. The accuracy of this model strongly depends on the finess of the mesh; however, a fine discretization with a large grid number dramatically increases the computational time. So an efficient numerical scheme is of vital importance in applying this model to simulate the slider-disk contact.

## 3. Numerical schemes for solving the linear system

Johnson [14] described two numerical methods – a matrix inversion method and a variational method – to solve the linear system, which is produced by the contact model based on influence coefficients for the normal pressure. In fact, almost all papers on the contact model based on influence coefficients uses one of these two numerical schemes, for example, [37][38][39][40]. Here we modify these two numerical methods and make them suitable for the simulation of slider-disk contact.

a) Conjugate Gradient (CG) method

The problem of the slider-disk contact is to find the contact regions with known contact pressure $p$ for a certain slider disk gap $h$. A first approximation to the contact regions is the geometry overlap regions, i.e., all the nodes in contact regions are {*Node i:*

$h_i<0\}$. Then the CG method instead of matrix inversion is used to solve the linear equations,

$$\sum_{j\in \text{Contact Region}} C_{ij} p_j = -h_i , \tag{15}$$

or in a matrix form, $[C]\{p\} = -\{h\}$.

The solution of Equation (15) may have pressure elements at some nodes with negative values, which implies that a tensile traction is required at those nodes to maintain contact over the entire assumed contact region. Then a new approximation to the contact region can be taken as the former region without those negative pressure nodes. Repeat this step and refine the approximation of the contact regions until convergence to a set of positive pressure elements is achieved. The obtained solution may have pressure elements at some nodes larger than the hardness H. Then we change the values of these pressure elements to H. With this modified pressure distribution and Equation (14), i.e.

$$\sum_{j\in \text{Contact Region}} C_{ij} p_j \begin{cases} = -h_i, & \text{then i is in the new appxoimation to the contact region} \\ > -h_i, & \text{the i is out of new approximation to the contact region} \end{cases},$$

a new approximation to the contact region can be calculated. Then we repeat the steps mentioned above until all of the pressure elements have values between 0 and H. The algorithm is illustrated in Fig. 8.

The CG method itself is an iterative scheme that generates a sequence of approximations of the solution from an arbitrary initial approximation [32]. The method is represented by the following recurrence formulas,

$$\{p^{(s+1)}\} = \{p^{(s)}\} + \frac{\{f^{(s)}\}^T\{t^{(s)}\}}{\{t^{(s)}\}^T[C]\{t^{(s)}\}}\{t^{(s)}\}$$

$$\{f^{(s+1)}\} = \{f^{(s)}\} - \frac{\{f^{(s)}\}^T\{t^{(s)}\}}{\{t^{(s)}\}^T[C]\{t^{(s)}\}}[C]\{t^{(s)}\}$$

$$\{t^{(s+1)}\} = \{f^{(s+1)}\} + \frac{\{f^{(s+1)}\}^T\{f^{(s+1)}\}}{\{f^{(s)}\}^T\{f^{(s)}\}}\{t^{(s)}\}$$

where $s = 0,1,2,...$ is the step number. $\{t\}$ and $\{f\}$ are vectors of the same size as the pressure vector $\{p\}$ . The starting pressure vector $\{p^{(0)}\}$ is arbitrary and $\{t^{(0)}\} = \{f^{(0)}\} = -\{h\} - [C]\{p^{(0)}\}$.

b) Gradient Projection Conjugate Gradient (GPCG) method

Mathematically the solution of the linear equations $[K]\{a\} = \{b\}$ is also the solution that minimizes the convex function $\Pi(\{a\}) = \frac{1}{2}\{a\}^T[K]\{a\} - \{a\}^T\{b\}$ if $[K]$ is a positive definite matrix. So obtaining the solution $\{p\}$ of the linear systems formed by the influence coefficient matrix, i.e. $[C]\{p\} = -\{h\}$ , is equivalent to minimizing the function $f(\{p\}) = \frac{1}{2}\{p\}^T[C]\{p\} + \{h\}^T\{p\}$ if $[C]$ is a positive definite matrix, which is the case for a uniform mesh (the adaptive mesh is analyzed later). And the iterations in the CG method to obtain a solution $\{p\}$ with all components bounded by 0 and H are equivalent in effort to that required to minimize the function $f(\{p\}) = \frac{1}{2}\{p\}^T[C]\{p\} + \{h\}^T\{p\}$ within a bounded region [*0, H*] for all components.

It was shown by Kalker [41] that the true contact area and distribution of surface tractions minimize the total complementary energy $V^*$,

$$V^* = \frac{1}{2} \int_{\text{contact region}} p(\bar{u}_{z(s)} + \bar{u}_{z(d)i}) ds + \int_{\text{contact region}} phds \tag{16}$$

Using a uniform mesh to discretize all function, Equation (16) can be expressed as,

$$\begin{aligned} V^* &= \frac{1}{2} \sum_{i,j \in \text{contact region}} s_i p_i C_{ij} p_j + \sum_{j \in \text{contact region}} s_i p_i h_i \\ &= s(\frac{1}{2} \sum_{i,j \in \text{contact region}} p_i C_{ij} p_j + \sum_{j \in \text{contact region}} p_i h_i) \\ &= sf(\{p\}) \end{aligned} \tag{17}$$

Equation (17) suggests the equivalence between minimizing $V^*$ and minimizing the function $f(\{p\})$. The object function for minimization in the case of an adaptive mesh is discussed later.

We can still use the geometric overlap regions, which have all the nodes in the contact region {Node $i$: $h_i$<0}, as a first approximation to the contact area. Then the slider-disk contact problem becomes a standard quadratic minimization problem with simple bound constraints. Here we propose to use the GPCG method to deal with the quadratic minimization. The GPCG method was developed by More and Toraldo in 1991 [42]. It uses the conjugate gradient method to explore one active set of constraints and the gradient projection method to move to a new active set. It combines a multiple activation/inactivation strategy of gradient projection with the finite termination property of the CG method. It works efficiently for large-scale bound-constrained quadratic programming problems with a small number of iterations and a small number of function-gradient evaluations and Hessian vector products per iteration.

The GPCG method starts from an arbitrary initial approximation. At each iteration the inputs of the GPCG method are,

Function evaluation: $\frac{1}{2}\{p^{(s)}\}^T[C]\{p^{(s)}\}+\{h\}^T\{p^{(s)}\}$

Gradient evolution: $[C]\{p^{(s)}\}+\{h\}$

Hessian-vector production: $[C]\{p^{(s)}\}$

Obviously both the CG method and the GPCG method require a large number of matrix-vector products. This is the reason why both of these two algorithms are time-consuming for larger scale contact problems, where the number of contacting nodes may be as large as $10^3$ in CML dynamic simulations.

c) Uniform mesh

If the slider and its projection on the disk surface are discretized with a uniform mesh, the FFT method is usually used to improve the computation speed [37, 38, 39, and 40]. All grids are the same size for a uniform mesh. Thus the influence coefficient is only a function of relative position, which means $C_{ij}=C_{ji}$ and $C_{ij}=C(m-k,n-l)$, where (*m, n*) and (*k, l*) are the coordinates of node *i* and node *j* in the x-y frame shown as Fig. 5, respectively. The total elastic strain energy is always positive for nonzero pressure distribution, i.e.

$$0\le U=\frac{1}{2}\int_{\text{contact region}} p(\bar{u}_{z(s)}+\bar{u}_{z(d)i})ds=\frac{1}{2}\sum_{i,j\ \in\ \text{contact region}} s_i p_i C_{ij} p_j=\frac{1}{2}s\sum_{i,j\ \in\ \text{contact region}} p_i C_{ij} p_j ,$$

where *s* is the grid area. This ensures that the influence coefficient matrix is positive definite. So the convergence of the CG method or the GPCG method is ensured. Notice that each iteration in the CG or the GPCG method involves a large number of computations of the product of the influence coefficient matrix and a pressure vector. We have the coefficient matrix $C_{ij}=C(m-k,n-l)$, and the pressure element at node *j*

$p_j = p(k,l)$, which can be rewritten as a matrix $[p(k,l)]$ and the slider-disk gap at node *i*, $h_i = h(m,n)$, which can also be rewritten as a matrix $[h(m,n)]$. Then we have,

$$\sum_i C_{ij} p_j = -h_i \quad \Leftrightarrow \quad \sum_{k,l} C(m-k,n-l)\, p(k,l) = -h(m,n)$$

The summation of the multiplications on the left hand side of the second equation above has the form of a linear convolution. So the FFT (Fast Fourier Transform) can be used in the computation.

$$\sum_{k,l} C(m-k,n-l)\, p(k,l) = IFFT(FFT([C]) \bullet FFT([p])),$$

where $\bullet$ is the operation of element -by-element multiplication.

There are two numerical ways for applying the FFT to contact analysis. The general processes are simply sketched here. One way is based on the Continuous Convolution Theorem [38]. First, we use the FFT to transform the pressure vector to the frequency domain. Second, we calculate the influence coefficient matrix directly in the frequency domain with the Fourier-transformed Papkovich-Neuber potentials. Third, we multiply each component of the $FFT([p])$ with the influence coefficient matrix at the corresponding frequency. Forth, we compute the inverse FFT to obtain the displacement matrix. The other way is based on the Discrete Convolution Theorem [43]. It is similar to the first way at the first step and the last step. But at the second step it calculates the discrete influence coefficient matrix in the space domain and then uses the discrete FFT to transform the coefficient matrix to the frequency domain. Then at the third step it does an element-by-element multiplication of the matrix $FFT([C])$ and $FFT([p])$. Notice that here the pressure vector $\{p\}$ is not a periodic function. A periodic error occurs if $\{p\}$ is extended periodically for the purpose of computing the FFT. Some techniques have been

developed to improve the accuracy of the FFT in contact analysis [39] [40] [43] [44]. However, all of them require the computational domain to be much larger than the target domain, resulting in a decrease of calculation efficiency.

d) Adaptive mesh

No publication was found that performed contact analysis based on an adaptive mesh. In an adaptive mesh all of the grids are not the same size, which means that $C_{ij}$ depends on the size of the grid at node j as well as the position of node i relative to node j. In this case, $C_{ij} \neq C_{ji}$ and the matrix-vector multiplication cannot be transferred to a convolution form. So the FFT cannot be used to speed up the computation of the matrix-vector multiplication. To make sure that the CG and the GPCG method still converge, we make some changes in the influence coefficient matrix for the CG method and the GPCG method for use with adaptive meshes.

Notice that $[C]\{p\} = -\{h\} \Leftrightarrow [C]^T[C]\{p\} = -[C]^T\{h\}$. So in the CG method we solve $[C]^T[C]\{p\} = -[C]^T\{h\}$, where $[C]^T[C]$ is a symmetric and positive definite matrix, instead of $[C]\{p\} = -\{h\}$. In fact this is called the CG squared method. Also the Bi-conjugate Gradient method can be used for the original non-symmetric linear system.

The total complementary energy is,

$$
\begin{aligned}
V^* &= \frac{1}{2} \sum_{i,j \in \text{contact region}} s_i p_i C_{ij} p_j + \sum_{j \in \text{contact region}} s_i p_i h_i \\
&= \frac{1}{2} \sum_{i,j \in \text{contact region}} \frac{1}{2}(s_i p_i C_{ij} p_j + s_j p_j C_{ji} p_i) + \sum_{j \in \text{contact region}} s_i p_i h_i \\
&= \frac{1}{2} \sum_{i,j \in \text{contact region}} p_i \frac{(s_i C_{ij} + s_j C_{ji})}{2} p_j + \sum_{j \in \text{contact region}} p_i h_i s_i
\end{aligned}
$$

Let $C'_{ij} = \dfrac{(s_i C_{ij} + s_j C_{ji})}{2}$, $h'_i = h_i s_i$. Then we have $C'_{ij} = C'_{ji}$, and

$$V^* = (\frac{1}{2} \sum_{i,j \in \text{contact region}} p_i C'_{ij} p_j + \sum_{j \in \text{contact region}} p_i h'_i)$$

The total elastic strain energy is positive for any nonzero pressure distribution,

$$0 \le U = \frac{1}{2} \int_{\text{contact region}} p(\overline{u}_{z(s)} + \overline{u}_{z(d)i}) ds = \frac{1}{2} \sum_{i,j \in \text{contact region}} s_i p_i C_{ij} p_j = \frac{1}{2} \sum_{i,j \in \text{contact region}} p_i C'_{ij} p_j \ .$$

So the matrix $\left[C'_{ij}\right]$ is symmetric and positive definite. Thus we can use this $\left[C'_{ij}\right]$ instead of $\left[C_{ij}\right]$ in the GPCG method.

In the CML air bearing simulation an adaptive grid generation scheme based on the air pressure gradient is used to numerically solve the Reynolds Equation [33]. In this adaptive mesh the grid density is higher at the ABS where the flying height is lower. Those places with lower flying height are more likely to have contact with the disk. So this adaptive mesh can be used to analyze the slider-disk contact in the slider dynamic simulation. This avoids introducing a new mesh for the slider dynamic simulation.

**5. Computation time for the CG method and the GPCG method**

The computation time of the CG method or the GPCG method is related to the size of the first approximation of the contact regions, i.e. the number of nodes in the geometrical overlap regions. The time consumption versus the node number is plotted in Fig. 6 for the CG method and the GPCG method. It is obvious that the GPCG method converges faster than the CG method. The reason may be that the GPCG method has a smaller number of iterations and less matrix-vector multiplications per iteration. So we propose to use the GPCG method in the CML dynamic simulation.

**6. Comparison of the contact model based on influence coefficients and the multi-asperity contact model by Cha**

Cha and Bogy [1] proposed a multi-asperity contact model, which is used in the current CML air bearing simulation program for the slider-disk impact when $d<0$. This multi-asperity contact model is based on Chang and Ling's elastic-plastic model [9]. This model considers the hysteresis between the loading and unloading process. In the unloading process, only the elastic strain energy is released. In Cha's model each contacting node is a part of a spherical asperity whose radius is calculated through the contact interferences of four nearest neighboring nodes. This model is accurate for Hertzian contact but it may give incorrect results for non-Hertzian contact. Here we do numerical simulations for two cases using this multi-asperity contact model and the new contact model based on influence coefficients. The first case has a flat rigid slider in contact with a spherical asperity on the disk surface, as shown as Fig. 7(a). The equivalent Young's modulus $E^*$ is 85.29GPa and the maximum interference is 2.0μm. The asperity radius is 2.0μm. Since the Young's modulus is high and the interference is only on the order of μm, the bulk deformation of the disk is negligible. So this case is very close to Hertzian contact. The second case is a rigid slider with a flat pad in contact with a smooth disk, as shown in Fig. 7(b). This is non-Hertzian contact. The equivalent modulus E* is 85.29GPa and the interference is 2.0um. Simulation results of the influence coefficient model, Cha's model and the analytical solution are shown in Table II (a) and II (b), respectively. It is seen that with more nodes the contact model based on influence coefficients gives a more accurate result. And Cha's model produces a wrong result for non-Herzian contact.

## CONCLUSION

The GW model is proved to be the simplest and a sufficiently accurate model for the slider-disk asperity contact, while the KE model can give slightly more accurate results at the cost of computation efficiency. The CEB model, which is used in the CML air bearing program, in fact can not give accurate contact results for the plasticity index $\Psi > 0.58$. When the slider crashes (the slider-disk gap is less than zero), these asperity-based contact models are no longer valid to model the slider-disk contact, since two of their pre-required assumptions may be violated. The contact model implemented here based on influence coefficients can be used for the slider-disk crash contact. The Gradient Projection Conjugate Gradient method is efficient in solving the linear system obtained from the contact model with the adaptive mesh generated by the air pressure gradient. The slider-disk contact may be non-Hertzian due to the ABS design and the arbitrary shape of the slider and disk surface profiles. In this case, Cha's [1] multi-asperity contact model may give an incorrect result for the slider-disk contact. Simulation of the dynamics of a partial contact head disk interface uses the analysis of slider-disk contact and impact in this report.

The effect of the pitch and roll angles in slider-disk contact simulations should be considered in the simulation. Pitch and roll are important effects in the slider-disk contact. The total contact force and contact area decreases dramatically as the pitch angle increases from 0 to 200urad. Approaches considering only the effect of the area of the contact pad on the total contact force may not be sufficiently accurate.

## ACKNOLEGEMENT

This research was supported by the Information Storage Industry Consortium (INSIC), the Computer Mechanics Laboratory (CML) at the University of California at Berkeley, and the National Science Foundation under Grant CMS-0408484.

## REFERENCES

[1] Cha, E. and Bogy, D. B., 1995, "Numerical Simulation of Slider Interaction with Multiple Asperity Using Herzian Contact Model,", *ASME Jour. of Tribol.*, 117, pp.575-579.

[2] Iida, K. and Ono, K., 2003, "Design Consideration of Contact/Near-contact Sliders Based on a Rough Surface Contact Models", *ASME Jour. of Tribol.*, 125, pp. 562-570.

[3] Hu, Y., Jones, P. M., Chang, P. T. and Bogy, D. B., 1998, "Partial contact air bearing characteristics of tripad sliders for proximity recording," *ASME Jour. of Tribol.*, 120, pp.272-279.

[4] Bogy, D. B., Stanley, H. M., Donovan, M. and Cha, E., 1993, "Some Critical Tribological Issues in Contact and Near-Contact Recording", *IEEE Trans. On Magnetics*, 29, pp.230-234.

[5] Ono, K., Yamamura, Y. and Mizokoshi, T., 1995, "Computer Analysis of the Dynamic Contact Behavior and Tracking Characteristics of a Single-Degree-of-Freedom Slider Model for a Contact Recording Head," *ASME Jour. of Tribol.*, 117, pp.124-129.

[6] Greenwood, J. A., and Williamson, J. B. P., 1966, "Contact of Nominally Flat Surfaces," *Proc. Roy. Soc. (London)*, A295, pp. 300-319.

[7] Chang, W. R., Etsion, I. and Bogy, D. B., 1987, “An Elastic-plastic Model for the Contact of Rough Surfaces,” *ASME Jour. of Tribol.*, 109, pp 257-263.

[8] Kogut, L. and Etsion, I., 2003, “A Finite Element Based Elastic-Plastic Model for the Contact of Rough Surfaces,” *Trib. Trans.*, 46, pp 383-390.

[9] Chang, W. R. and Ling, F. F., 1992, “Normal Impact Model of Rough Surfaces,” *ASME Jour. of Tribol.*, 114, pp.439-447.

[10] Peng, W., Kiely, J. and Hsia, Y. T., 2005, “Wear Analysis of Head-Disk Interface During Contact,” *ASME Jour. of Tribol.*, 171, pp.171-179.

[11] Kral, E. R., and Komvopoulos, K., 1997, "Three-Dimensional Finite Element Analysis of Subsurface Stress and Strain Fields Due to Sliding Contact on an Elastic-Plastic Layered Medium," *ASME Jour. of Tribol.*, 119, pp. 332-341.

[12] Komvopoulos, K. and Ye, N., 2002, “Elastic-Plastic Finite Element Analysis for the Head-Disk Interface with Fractal Topography Description”, *ASME Jour. of Tribol.*, 124, pp.775-784.

[13] Suh, A. Y. and Polycarpou, A. A, 2005, “Adhesive contact modeling for sub-5-nm ultralow flying magnetic storage head-disk interfaces including roughness effects,” *Journal of Applied Physics*, 97, pp.104328-104338.

[14] Johnson, K. L., 1985, *Contact Mechanics*, Cambridge University Press, Cambridge, UK.

[15] Greenwood, J. A., and Tripp, J. H., 1971, “The Contact of Two Nominally Flat Rough Surfaces,” *Proc. Instn. Mech. Engrs.*, 185, pp.625-633.

[16] Abbott, E. J. and Firestone, F. A., 1933, “Specifying Surface Quality- a Method Based on Accurate Measurement and Comparison,” *Mech. Eng.*, 55, pp 569-573.

[17] Evseev, D. G., Medvedev, B. M. and Grigoriyan, G. G., 1991, "Modification of the Elastic-plastic Model for the Contact of Rough Surfaces", *Wear*, 150, pp 79-88.

[18] Chang, W. R., 1997, "An Elastic-plastic Contact Model for a Rough Surface with an Ion-plated Soft Metallic Coating," *Wear*, 212, pp 229-237.

[19] Zhao, Y., Maietta, D. M. and Chang, L., 2000, "An Asperity Microcontact Model Incorporating the Transition from Elastic Deformation to Fully Plastic Flow," *ASME Jour. of Tribol.*, 122, pp 86-93.

[20] McCool, J. I., 1986, "Predicting Microfracture in Ceramics via a Micro-contact Model," *ASME Jour. of Tribol.*, 108, pp. 380-386.

[21] Horng, J. H., 1998, "An Elastic-plastic Microcontact Model for rough surfaces," *ASME Jour. of Tribol.*, 120, pp.82-88.

[22] Kogut, L. and Etsion, I., 2000, "The Contact of a Compliant Curved and a Nominally Flat Rough Surfaces," *Trib. Trans.*, 43, pp. 507-513.

[23] Yu, N. and Polycarpou, A. A., 2002, "Contact of Rough Surfaces with Asymmetric Distribution of Asperity Heights", *ASME Jour. of Tribol.*, 124. pp. 367-376

[24] Jackson, R. L. and Green, I, 2003, "A Statistical Model of Elasto-plastic Asperity Contact of Rough Surfaces," *Proceedings of 2003 STLE/ASME Joint International Tribology Conference*.

[25] McCool, J. I., 1987, "Relating Profile Instrument Measurements to the Functional Performance of Rough Surfaces", *Trans. of the ASME*, pp. 264-270

[26] Nayak, P. R., 1973, "Random Process Model of Rough Surface," *J. of Lubric. Tech.*, 93(3), pp. 398-407.

[27] Sayles, R. S., and Thomas, T.R., 1978, "Surface Topography as a Nonstationary Random Process", *Nature*, 271, pp. 431-434.

[28] Majumdar, A. and Bhushan, B., 1990, "Role of Fractal Geometry in Roughness Characterization and Contact Mechanics of Surfaces," *ASME Jour. of Tribol.*, 112, pp. 205-216.

[29] Majumdar, A. and Bhushan, B., 1991, "Fractal Model of Elastic-Plastic Contact between Rough Surfaces", *ASME Jour. of Tribol.*, 113, pp. 1-11.

[30] Yan, W. and Komvopoulos, K., 1998, "Contact Analysis of Elastic-plastic Fractal Surfaces," *Jour. of Applied Physics*, 84, pp.3617-3624.

[31] Chung, J. C. and Lin, J. F., 2004, "Fractal Model Developed for Elliptical Elastic-Plastic Asperity Microcontacts of Rough Surfaces," *ASME Jour. of Tribol.*, 126, pp.646-654.

[32] Press, W. H., Teukolsky, S. A., Wetterling, W. T., and Flannery, B. P., 1999, *Numerical Recipes in FORTRAN, the art of Scientific Computing*, 2nd ed., Cambridge University Press, Cambridge, UK.

[33] Lu, S., 1997, "Numerical Simulation of Slider Air Bearings", Ph.D. Thesis, University of California at Berkeley.

[34] Zhao, Y. and Chang, L., 2001, "A Model of Asperity Interactions in Elastic-Plastic Contact of Rough Surfaces", *ASME Jour. of Tribol.*, 123, 857-864.

[35] Love, A. E. H., 1929, "Stress produced in a semi-infinite solid by pressure on part of the boundary", *Proc. Roy. Soc. (London)*, A228, pp. 377-420.

[36] Shi, F. H., and Wang, Q., 1998, "A Method of influence functions for thermal analyses of tribological elements," *Tribol. Trans.*, 41, pp.350–358.

[37] O'Sullivan, T. C. and King, R. B., 1988, "Sliding Contact Stress Field Due to a Spherical Indenter on a Layered Elastic Medium," *ASME Jour. of Tribol.*, 110, pp. 235-240.

[38] Nogi, T. and Kato, T., 1997, "Influence of a Hard Surface layer on the Limit of Elastic Contact; Part I- Analysis Using a Real Surface Model," *ASME Jour. of Tribol.*, 119, pp.493-500.

[39] Ai, X. L. and Sawamiphakdi, K., 1991, "Solving Elastic Contact Between Rough Surfaces as an Unconstrain Strain Energy Minimization by Using CGM and FFT techniques," *ASME Jour. of Tribol.*, 120, pp.668-676.

[40] Polonsky, I. A. and Keer, L. M., 2000, "A Fast and Accurate Method for Numerical Analysis of Elastic Layered Contacts," *ASME Jour. of Tribol.*, 121, pp. 668-679.

[41] Kalker, J. J., 1977, "Variational Principles of Contact Elastostatics", *Journ. Inst. Math. & Appl.*, 20, pp.199-219.

[42] More, J. J. and Toraldo, G., 1991, "On the solution of large quadratic programming problems with bound constraints,"*SIAM J. Optimization*, 1, pp. 93 – 113.

[43] Liu, S. B., Wang, Q. and Liu, G., 2000, "A Versatile Method of Discrete Convolution and FFT (DC-FFT) for contact Analysis," *Wear*, 243, pp. 101-110.

[44] Liu, S. B. and Wang, Q., 2002, "Studying Contact Stress Fields Caused by Surface Traction with a Discrete Convolution and Fast Fourier Transform Algorithm," *ASME Jour. of Tribol.*, 124, pp. 36-45.

Table I Slider and disk roughness and material parameters

| Individual Surfaces | Disk 1 | Disk 2 | Disk 3 | Slider |
|---|---|---|---|---|
| $\sigma$ (nm) | 1.486 | 1.066 | 0.123 | 0.643 |
| $R$ (μm) | 3.765 | 8.431 | 14.204 | 7.147 |
| $\eta$ ($\mu m^{-2}$) | 7.071 | 5.683 | 18.163 | 8.849 |
| | | | | |
| Combined surfaces | Case 1: Slider/Disk 1 | Case 2: Slider/Disk 2 | Case 3: Slider/Disk 3 | |
| $\sigma$ (nm) | 1.619 | 1.245 | 0.654 | |
| $R$ (μm) | 3.331 | 5.452 | 6.384 | |
| $\eta$ ($\mu m^{-2}$) | 7.393 | 7.177 | 9.871 | |
| $\sigma_s$ (nm) | 1.417 | 1.143 | 0.578 | |
| $y_s$ (nm) | 1.866 | 1.174 | 0.729 | |
| $\psi$ | 0.836 | 0.587 | 0.386 | |
| | | | | |
| Material Properties | | | | |
| $v_d$ and $v_s$ | 0.20, 0.21 | | | |
| $E_d$ and $E_s$ (Gpa) | 100, 450 | | | |
| $E$ (Gpa) | 85.29 | | | |
| $H$ (Gpa) | 2.5 | | | |

Table II Numerical results for two cases of slider-disk contact shown in Fig. 7

(a)

| | Contact Force | Contact Area |
|---|---|---|
| New Model (9 nodes) | $5.277X10^{-6}$ N | $7.177X10^{-15}$ $m^2$ |
| New Model (261 nodes) | $5.087X10^{-6}$ N | $6.482X10^{-15}$ $m^2$ |
| Cha ‘s Model [7] | $5.086X10^{-6}$ N | $6.283X10^{-15}$ $m^2$ |
| Analytical Solution | $5.086X10^{-6}$ N | $6.283X10^{-15}$ $m^2$ |

(b)

| | Contact Force | Contact Area |
|---|---|---|
| New Model (5 nodes) | $3.010X10^{-6}$ N | $1.118X10^{-15}$ $m^2$ |
| New Model (49 nodes) | $3.291X10^{-6}$ N | $1.217X10^{-15}$ $m^2$ |
| Cha ‘s Model [7] | 0 N | 0 $m^2$ |
| Analytical Solution | $3.416X10^{-6}$ N | $1.257X10^{-15}$ $m^2$ |

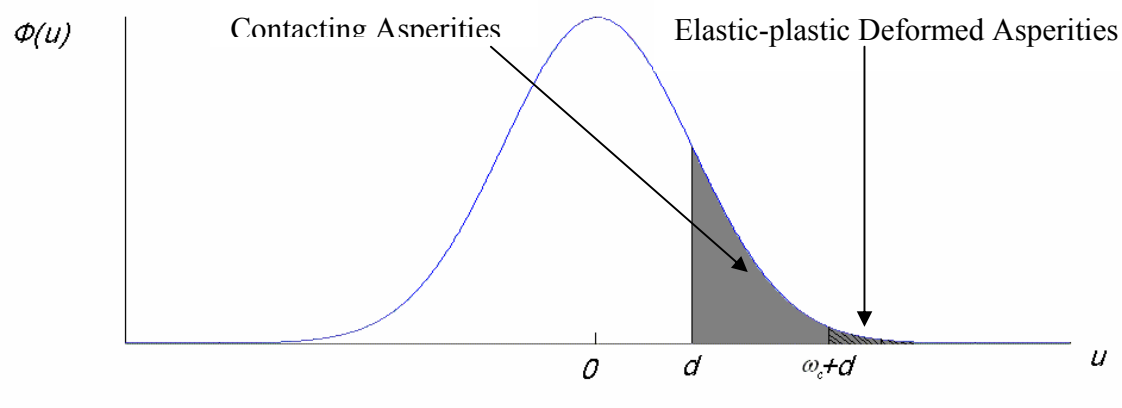


Fig. 1 Density function of Gaussian distributed asperity height *u*

Case 1: $\psi = 0.836$

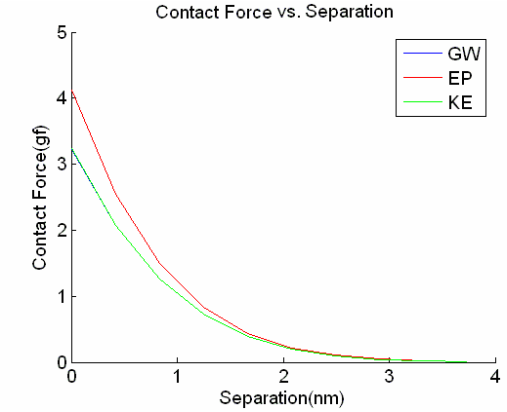


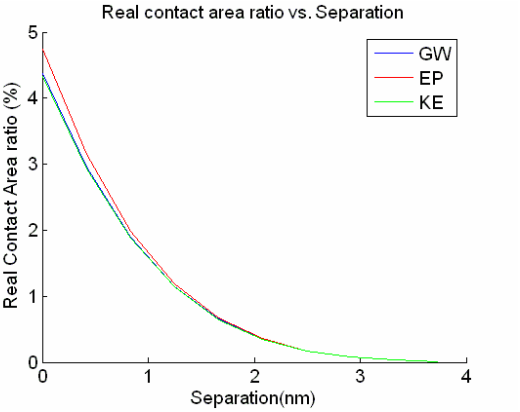


Case 2: $\psi = 0.587$

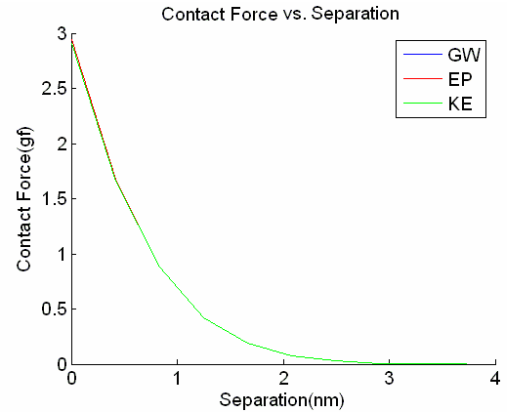


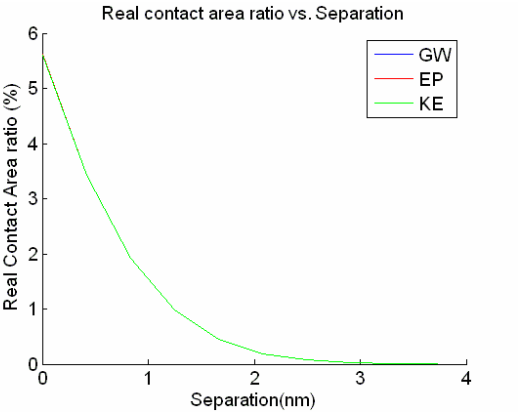


Case 3: $\psi = 0.386$

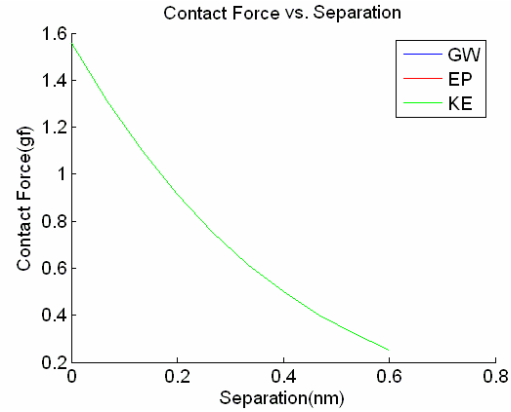


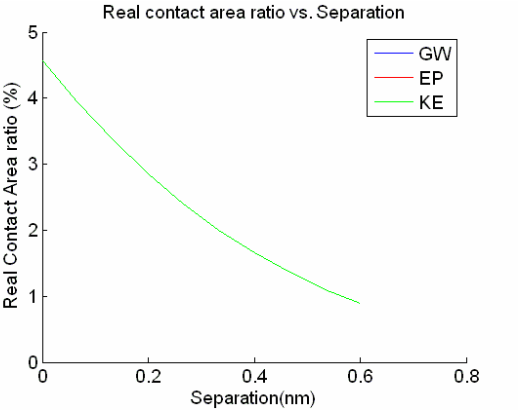


Fig. 2 Contact Force separation and real contact area ratio for three cases with GW model, EP model (i.e. CEB model) and KE model

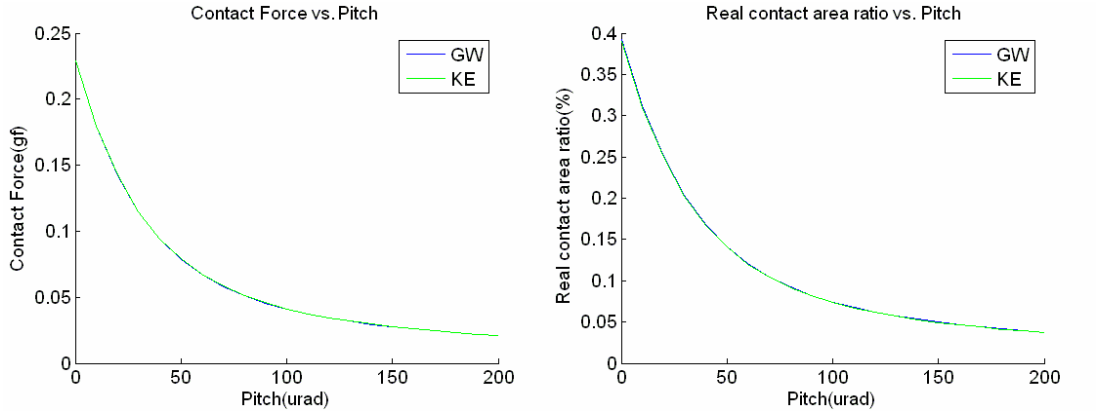


Fig. 3 Contact force and real contact area for various pitch angles

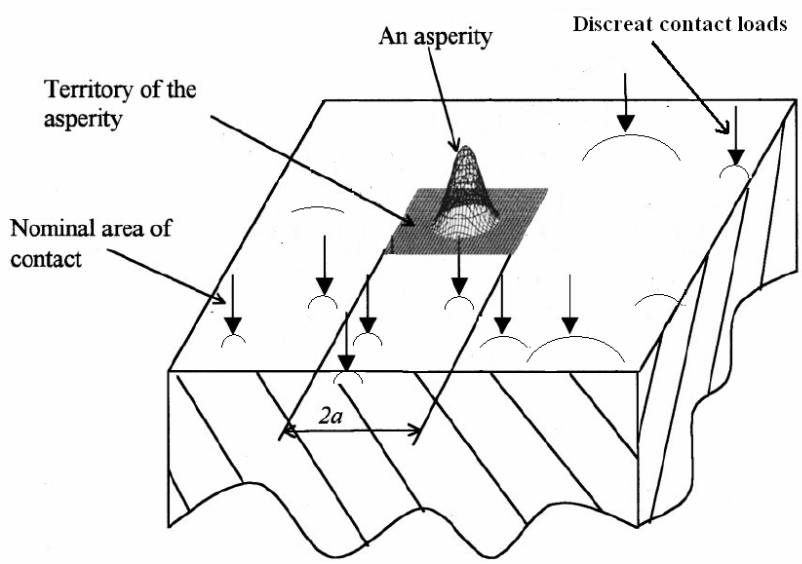


(a) The deformation at a given asperity due to pressures at all other contacting asperities

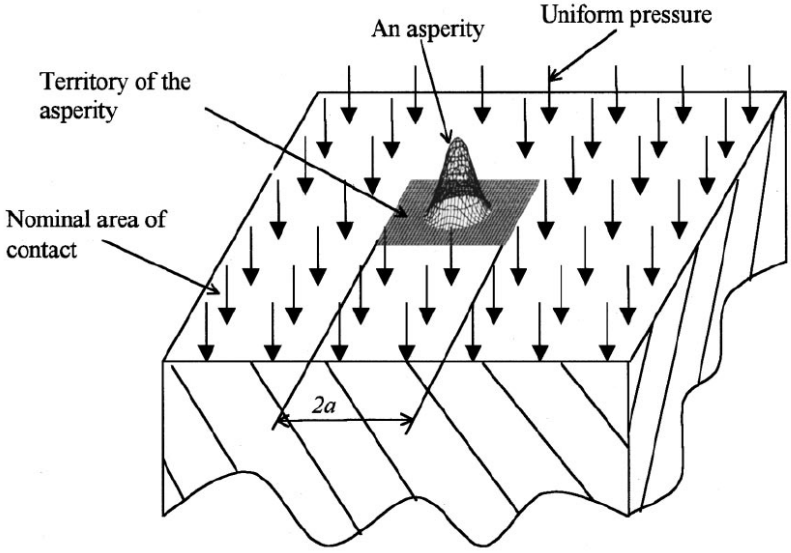


(b) The deformation at a given asperity due to an equivalent uniform pressure applied over the surface area outside the territory of the asperity [34]

Fig. 4 Two different questions that can not be related through Saint-Venant's Principle

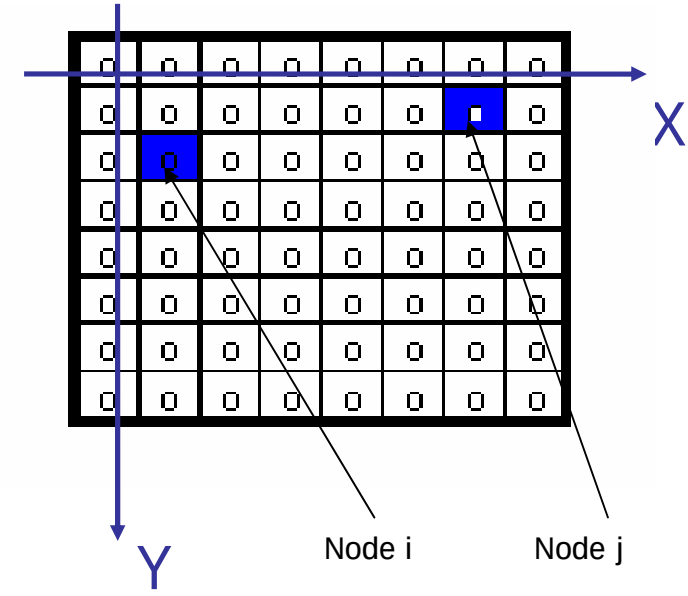


Fig. 5 Demonstration of meshed slider surface

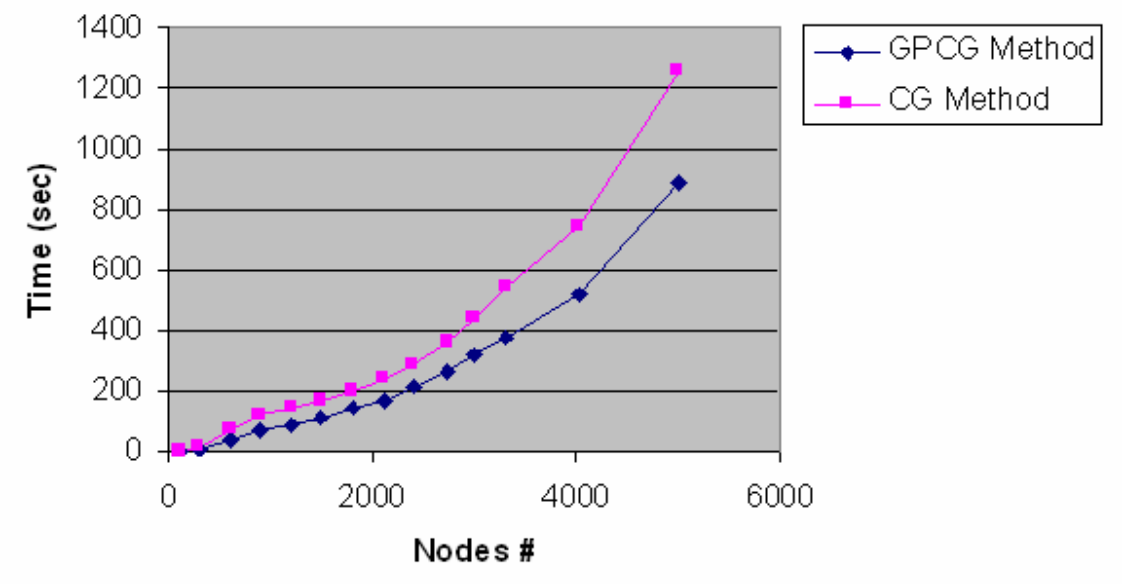


Fig. 6 Time consumption of CG method and GPCG method

(a) A flat rigid slider in contact with a spherical asperity on the disk surface

(b) A rigid slider with a flat pad in contact with a smooth disk

Fig. 7 Two slider-disk contact cases

(a) CG method

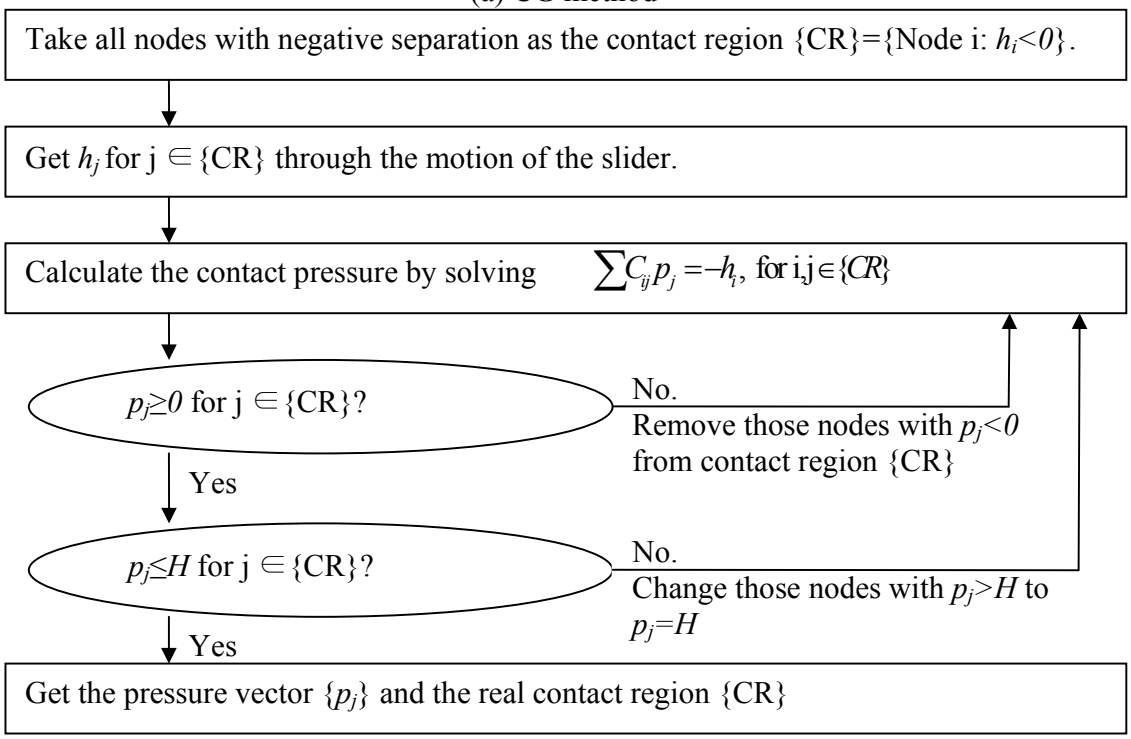


(b) GPCG method

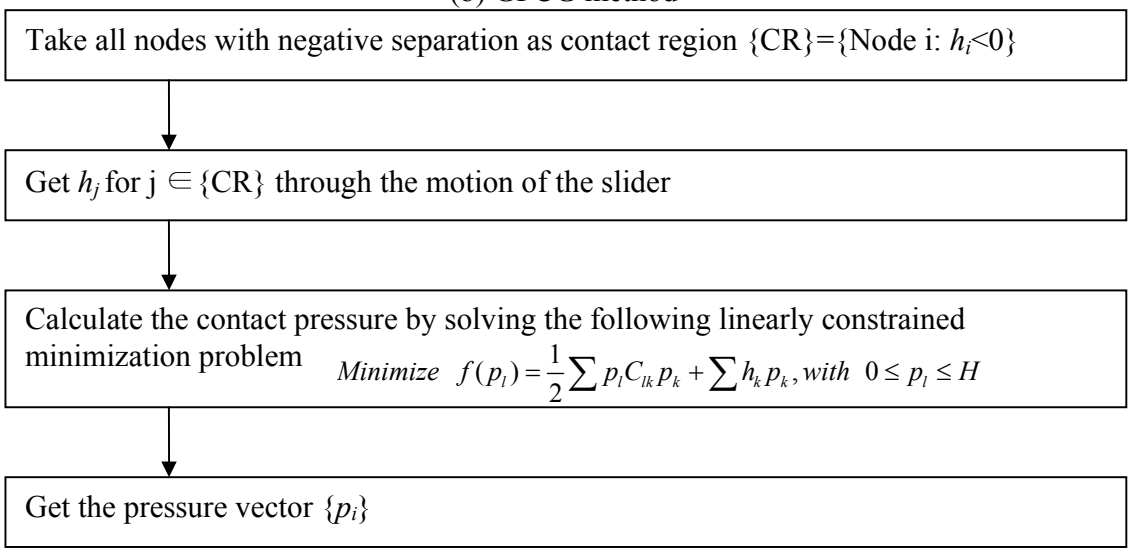


Fig. 8 Algorithms of two numercial skemes for contact analysis with the influcent coefficient model.